Charge Transfer Device Star Tracker Applications

R. A. Deters* and R. L. Gutshall†
Ball Aerospace Systems Division, Boulder, Colorado

The physical and functional advantages of solid-state charge transfer devices as detectors in star trackers have been evident for several years. In addition to high accuracy in a wide field of view, the versatility of the charge transfer device combination to incorporate various acquisition and tracking algorithms has been demonstrated in breadboard sensors. The charge transfer detector tracker overcame the lack of a flight pedigree as part of the Solar Array Experiment flown on Space Transportation System mission 41D in August 1984. The Retroreflector Field Tracker accurately measured the position of 23 reflective targets on the solar array to provide deflection data for structural analysis. This successful mission in space demonstrates the capability for use of charge-transfer-device star trackers in many space applications. The present workhorse, which provides reasonable accuracy in a wide field of view, is the image dissector tube standard star tracker. A charge transfer device standard star tracker will provide superior performance with power, weight, volume, and peripheral support savings. More significantly, it offers the flexibility to satisfy many performance requirements anticipated for pointing control and attitude determination of future spacecraft.

Introduction

SINCE the mid-1970s, the solid-state charge transfer device (CTD) has been hailed as the detector to replace the image dissector tube in star sensors. The CTD, an array of photosensitive picture elements, or pixels, formed through the use of integrated circuit processing techniques, has overwhelming physical and functional advantages over the image dissector tube (IDT). Functionally, the CTD has a wider spectral response that increases the stellar sensitivity by 20%; the photon-generated signal is integrated and stored at the respective pixels until removed by command. Physically, the CTD is a semiconductor chip mounted on a thermoelectric cooler (for most applications) interfacing with low-voltage drive and signal amplifiers. The IDT is a glass tube surrounded with focus coil, deflection coil, and magnetic shields and operates at voltages of at least 2000 V. As illustrated in Fig. 1, the difference in size is dramatic between IDT trackers and CTD trackers that meet identical performance parameters.

The primary advantage of the IDT is its design maturity which is based on many successful aerospace missions. With the application of calibration equations external to the tracker, accuracies of 0.2% of the field of view (FOV) have been continuously demonstrated. However, it is doubtful that additional calibration can sufficiently reduce error to meet the more stringent pointing requirements of upcoming missions. The CTD tracker can provide better accuracy at its output without the need for calibration. It is likely that future CTD systems will approach an accuracy of 10^{-5} of the FOV.

Typically, CTD's can be placed into one of two generic categories: 1) Charge coupled devices (CCD) and 2) Charge injection devices (CID). The main difference between the two is in the method of signal readout. The CCD is read out by sequential transfer of charge from pixel to pixel along each column. The charge signal, destructively removed, is synchronized with the pixel clocking. In a CID, each pixel or set of pixels may be directly accessed. Each pixel has a row- and column-connected capacitance between which charge can be transferred. This charge transfer allows a signal to be read out nondestructively, thus allowing multiple reads while charge is integrating on a pixel.

Either CTD provides the performance needed for a star tracker detector. However, certain capabilities of the CID make it better suited for star tracker applications.[1] A comparison of 15 parameters of the CID and CCD is presented in Table 1. The items that favor the CID for star tracker applications are:

1) Lower dark current (item 4) requires less cooling power;

2) Direct accessing (item 9) of only needed data requires less processing;

3) Operational flexibility (item 11) reduces system processing requirements and enhances performance; and

4) Lower power (item 12) reduces electrical and thermal design efforts.

The ST-256 CID, a detector developed specifically for star tracker applications, was chosen. The CID detector features low dark current and low variations from pixel-to-pixel dark current and response to background light. These favorable parameters simplify the algorithms required for achieving high accuracy. A radiation-hardening program for the CID detector has already demonstrated successful operation with no degradation of performance after exposure to 10^5 rad. Table 2 lists typical performance parameters of the ST-256, which were obtained through a test program conducted for NASA/MSFC[2] and are critical to system performance.

Laboratory Model CID Tracker

CID Operation

Figure 2 shows how a pixel is addressed on the CID array. Each pixel consists of column and row capacitors; charge is transferred between these capacitors.

Horizontal and vertical shift registers are located along two edges of the chip array. The registers control switches that are connected to the column and row conductors (capacitors). Four columns and four rows can be accessed simultaneously with the registers; the column drive lines (*E*-lines) provide interrogation of the desired column(s). Reading the preamplifier for the intersecting row allows a single pixel to be addressed. Row and column bias gates are

Presented as Paper 84-1851 at the AIAA Guidance and Control Conference, Seattle, WA, Aug. 20-22, 1984; received Jan. 31, 1985; revision received May 13, 1986.

*Electro-Optical Sensor Systems Engineer, High Technology Products. Member AIAA.

†Manager, Advanced Programs, High Technology Products.

provided (opposite the register) for single-line control of the full array.

The sum of a 4×4 block of pixels can be read by driving all four *E*-lines and reading the four preamplifier output voltages simultaneously. Data from a single pixel are acquired by driving one *E*-line and reading one preamplifier output. Charge injection is controlled by the bias gates.

A typical readout sequence is as follows:

1) The column and row biases are brought to zero to clear the entire array of stored charges by injection.

2) The row bias is set at −8 V and the column to −14 V for a read enable. The column potential "well," shown in Fig. 2, stores the photon-generated minority carriers.

3) Column and row biases are then floated, and the column is brought to zero via the *E*-lines. The collected charge is transferred to the row capacitor, and the displacement current causes a proportional row potential change that is sampled and held for processing.

Returning the column bias to −14 V and the row bias to −8 V transfers the charge back to the column capacitor, and another read cycle can be made. The accumulated charge is not lost, and repeating the read process would produce the same output plus the signal that had been collected during the first read period. This is the nondestructive readout (NDRO) cycle.

The multiple NDRO process available in the CID is an important feature in reducing fixed pattern and temporal readout noise. The fixed pattern noise is eliminated by taking two sets of samples for each reading and subtracting the first from the second. Although this results in a factor-of-two signal loss, the loss is more than recovered by summing NDRO's. In most applications of the CID detector in a star tracker, elimination of the pattern noise by subtraction of signals is preferred over use of a stored pattern map. The effective temporal noise is reduced by taking many samples for each of the first and second readings.

The signal-to-noise ratio (SNR) is a factor in the probability of acquisition of stars and the temporal uncertainty in position (noise equivalent angle) in the tracking of stars. The temporal noise is reduced by taking many samples for each of the first and second readings. The SNR is increased in proportion to the number of NDRO's raised to the 3/2 power.

Position Accuracy

Star trackers incorporate some method of modulation and signal processing to determine location of star image relative to a reference position on the detector. The CID, with its 256×256 individual charge integrating pixels, lends itself to a high degree of accuracy in determining the position of an image on its surface. This is accomplished by determining the pixel closest to the image center and then finding the relative displacement of the radiometric center from this pixel. The latter is accomplished with a centroiding algorithm that operates on the signals from the pixels encompassing the image. Since the interpolation is applied only to the position relative to the pixel nearest the star image center, a CID tracker has a resolution equivalent to the number of pixels divided by the interpolation accuracy. It is evident that accuracy could be improved either by increasing the number of pixels or by decreasing the interpolation error. Increasing the number of pixels while maintaining SNR requires optics changes which cause an exponential increase in complexity, size, weight, and power. Major emphasis has been placed on achieving the highest interpolation accuracy because it simplifies the tracker design.

Significant analysis has been performed, followed by testing of the effects of image differences on accuracy, because position interpolation is accomplished with a centroiding algorithm on the image spread function. An algorithm quite insensitive to image diameter provides less than 1% pixel accuracies. The feasibility of optics that will provide low chromatic aberrations over the wide CID response has been determined, and design of several different refractive lenses has been accomplished.

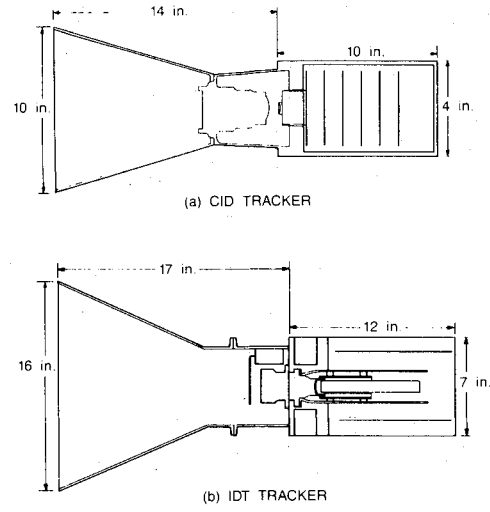

Fig. 1 CID and IDT trackers.

Table 1 CTD trade-off table

No.	Trade item	CID	CCD
1	Defect tolerance	+ Defects confined to pixel	− Defect propagates down columns
2	Optical overload tolerance	+ Blooming confined to local	− Blooming propagates down columns
3	Charge storage capacity	+ 10^6 carriers typical	+ 10^6 carriers typical
4	Dark current generation	+ 1 *nA* per cm^2 typical	− 5 *nA* per cm^2 typical
5	Quantum efficiency	+ High (0.4 to 1μ)	+ High (0.4 to 1μ)
6	Response uniformity	+ 0.6% rms typical	+ 1% rms typical
7	Temporal noise	+ 30 to 300 carriers typical	+ 50 to 200 carriers typical
8	Crosstalk sensitivity	+ Confined to adjacent pixel	− Occurs over several pixels
9	Data address	+ Direct *X-Y* access to data pixel	− "Bucket Brigade" to data pixel
10	Charge transfer efficiency	+ One transfer	− Full array transferred
11	Operational flexibility	+ Destructive or NDRO: on-chip processing	− Destructive full frame readout
12	Power	+ Only required pixels are read at required update rate	− Full array is read at required update rate
13	Radiation effects	+ Efficiency of only one transfer is affected	− Effects on transfer efficiency propagate down columns
14	Yield	+ Three masking operations involved in fabrication	− 5 to 12 masking operations involved in fabrication
15	Technical maturity	+ Implemented in tracker and tested	+ Implemented in tracker and tested

Test Results

The breadboard tracker, with characteristics listed in Table 3, was developed to verify the validity of the sensitivity and accuracy predicted by analysis. The tracket was implemented with a set of unique algorithms to perform the acquisition and track functions, although the objective of the majority of the tests was to verify position interpolation accuracy. Various tests have been conducted over the past six years. A summary of significant observations follows:

1) Tracking algorithms are developed that track a target moving at up to one pixel per update time. Tests verified tracking at rates greater than 5 pixels/s.

2) Interpolation algorithms are developed that routinely provide position accuracy at less than 3% of a pixel without calibration. These accuracies were demonstrated over a wide spectral range, with image size variations and different star intensities. Interpolation errors can be reduced to less than 1% of a pixel when the algorithm constants are adjusted for systematic characteristics of the pixel point spread response.

3) Tracking under constant rate conditions has an equivalent effect of changing the image diameter by smearing the deposited charge uniformly over the integration period. Other than a predictable lag in position output (because the mean position over the update time is computed rather than the instantaneous position at the end of update), no other error terms caused by rate were noted.

4) The response of the tracker to low-amplitude (roughly one pixel) target oscillations follows the sampling theorem $\sin x/x$ curve, with the update rate being the first null. Target motion is followed to about one-fourth the update rate, attenuated for higher frequencies, and integrated out completely for frequencies greater than ten times the update rate.

First Flight Application of a CID Tracker

The retroreflective field tracker (RFT) developed for the NASA Solar Array Experiment was the first application of a CID tracker in space. The RFT is an electro-optical position-measuring instrument that was part of the NASA-Marshall Space Flight Center Shuttle payload flown in August 1984 on STS Mission 41D. It measures the position of reflective targets on a 32-m (105-ft) solar array to provide data on the dynamics of motion for structural analysis of the large, flexible, lightweight array. As such, the RFT is a noncontact optical position sensor that could be used in applications such as large space structure alignment, rendezvous and docking, and surface figure control of large antennas.

The experiment concept is shown in Fig. 3, and significant physical and performance parameters for the RFT are listed in Table 4. The RFT illuminates, acquires, and tracks 23 retroreflective targets on the 3.7×32m solar array. Five pulsed infrared laser diode illuminators freeze the array motion, which has a maximum amplitude and maximum frequency of motion of 90 cm and 0.4 Hz, respectively. The return beams from the retroreflectors are focused and integrated on the CID detector. After the signal is read out, a nonilluminated integration is made and subtracted from the signal to remove constant background (e.g., sun and stray light).

An acquisition subarray of 12×12 pixels is moved across the detector, searching for targets. When one is detected, its position is compared to a stored target map for identification, track is maintained, and the target's position is added to the data output. After the FOV is completely searched in

Table 2 CID performance summary

Array size	256×256 pixels
Pixel size	20×20 μ
Dark current	$<10^4$ e^-/sec-pixel at 0°C
Quantum yield	>0.4
Dark current variation	$<1.5\%$
Response variation	$<1\%$
Readout noise	$<3.9e^-/\sqrt{\text{Hz}}$ read rate
Response point spread	Trapezoidal
Radiation tolerance	$>10^5$ rad

Table 3 Breadboard CID star tracker characteristics

CID array (ST-256)	256×256 pixels
Pixel size	20×20 μ
Lens EFL (Nikon f/2.8)	100 mm
Pixel angular subtense	41.253 arc sec
Tracker FOV	2.93×2.93 deg
Acquisition time	4 s (typical)
Position update	12 ms (bright stars) 1 s (dim stars)
Number of signal pixels for tracking	8 pixels
Projected position accuracy	0.01 pixel 0.4 arc sec for breadboard
Projected tracking rate without degradation in accuracy	0.5 pixel per update 20 arc sec per update for breadboard

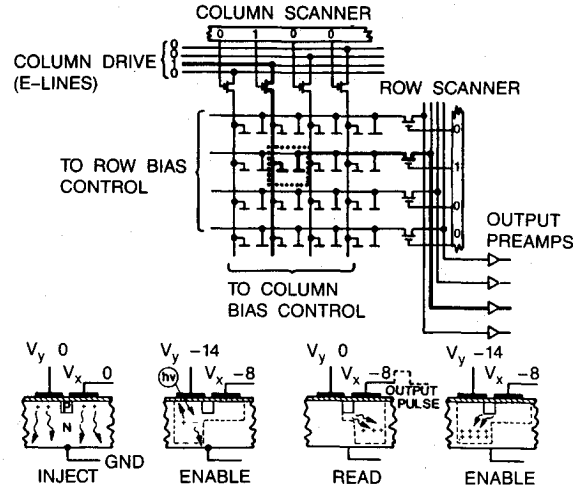

Fig. 2 Detector schematic.

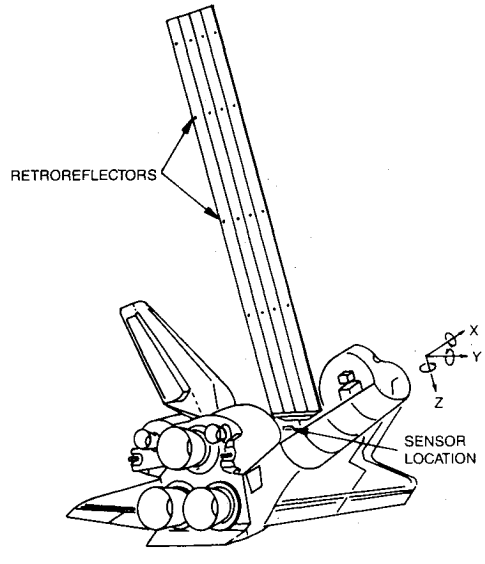

Fig. 3 Solar Array Experiment.

nominally 90 s, a "valid data" flag is set to allow the experiment to start recording data. If a target is lost, a search is made at the last known position to reacquire the target. The full detector search is continued to find targets missed during the initial acquisition or not reacquired within one track cycle using the multiple tracking capability of the CID detector. The 23 return images are tracked simultaneously at a rate of approximately 6 Hz. Each target position is interpolated to subpixel accuracy of 19 arc sec, 1σ (± 3 mm at 32 m), and referenced to sensor boresight angles. The interpolated position is generated at a 2-Hz rate and converted from sensor angle to orbiter coordinates for direct use by the experiment.

A block diagram of the RFT electronics, shown in Fig. 4, indicates the use of three Z80A microprocessors operating in parallel. One processor in the sensor head effects the acquisition and track function, along with controlling the laser diode timing. A processor in the main electronics implements the subpixel interpolation algorithm. It also maintains the target identification information list and performs the sensor-to-orbiter coordinate transformation. The last processor, also located in the main electronics, serves as the master control. It monitors orbiter signals, provides timing for the other processor functions, and serially outputs data to the experiment.

The focal plane (CID detector and associated electronics) used in the RFT is identical to that which can be used for star tracking applications. Operation of the RFT CID detector is similar to that described in other sections of this paper.

A CID Standard Star Tracker

Image dissector tube star trackers have been widely and successfully used since the 1960s.[3] Use of trackers as "strapped down" sensors, a practice that started in the early 1970s, required trackers with enough sensitivity to continuously track randomly encountered stars to an accuracy of 10 arc sec over a large FOV. The CT-401 star tracker[4] provided this capability for the Small Astronomy Satellite SAS-C and the High Energy Astronomical Observatory (HEAO-A and HEAO-C) and Magnetic Satellite (MAGSAT) spacecraft. The standard star tracker[5] (SST) provided the same sensitivity and accuracy for Solar Maximum Mission (SMM) and LANDSAT and is baselined for Space Telescope, Gamma Ray Observatory (GRO), and several other spacecraft. Any replacement for the SST must provide at least equal probability of tracking stars of opportunity with equal or better accuracy, anticipating future space vehicle requirements. Implementation of an SST using the CID detector provides more capability and versatility.

A CID star tracker that would provide equal or better performance than presently provided with the IDT SST is shown in Fig. 5. The CID SST is a two-package configuration, divided into a sensor and a processor, with the electronics divided as shown in Fig. 6. Although the configuration could be a single package, as shown in Fig. 1a, separation into two assemblies minimizes power dissipation in the sensor—a desirable feature since the CID detector must operate at less than 0°C. It also promotes better control of

Table 4 RFT parameters

Operational:
Tracks 23 targets simultaneously
Accuracy: ± 3 mm at 32m 1σ, (19 arc sec)
Target motion: ± 45 cm, 0 to 0.4-Hz Rate
Output data rate: 2 Hz
FOV: 22.5 deg × 22.5 deg
Laser diode illuminator system
Light shade protection angle (sun): ± 20 deg
Operation in full sunlight
Self-test
Environmental:
Shuttle launch loads: 21 Grms
Pressure: 10^{-7} Torr
Thermal:
-30°C to $+75$°C (nonoperating)
-15°C to $+20$°C (operating)
Internal heaters
no heat exchange with experiment
Physical:
Two-package design
13 mm f/1.8 Cine-Nikkor lens
ST-256 CID detector
Illuminator system uses five laser diodes with shaped output beams; the 20 mW lasers operate at 820 nm
Dimensions:
Head: 9.3 × 11.3 × 22.2 in.
Electronics: 9.7 × 8.5 × 15.5 in.
Weight: 52 lb
Power: 55W (excluding heaters) at 28 Vdc

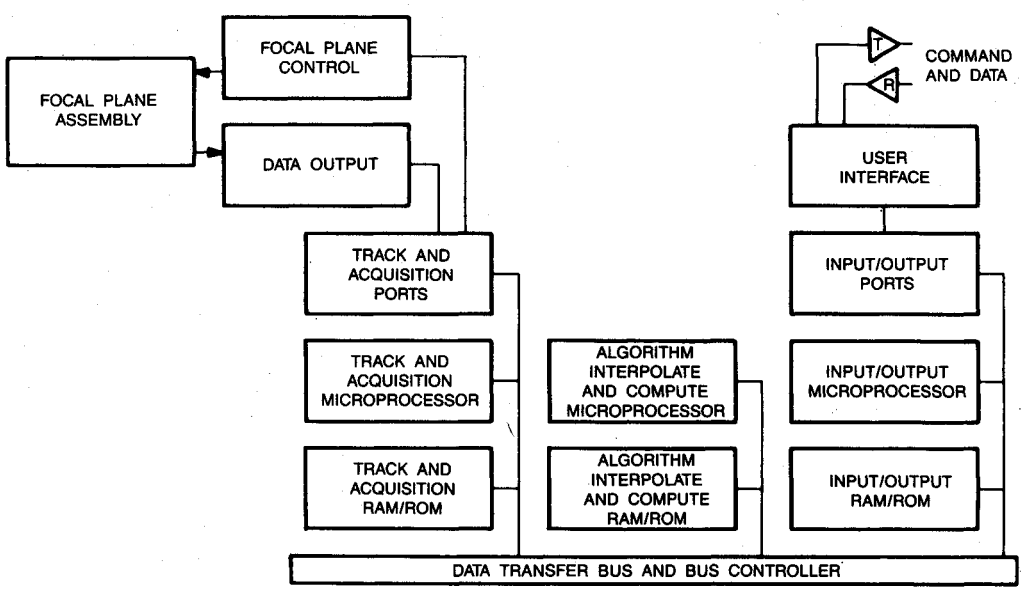

Fig. 4 RFT electronics.

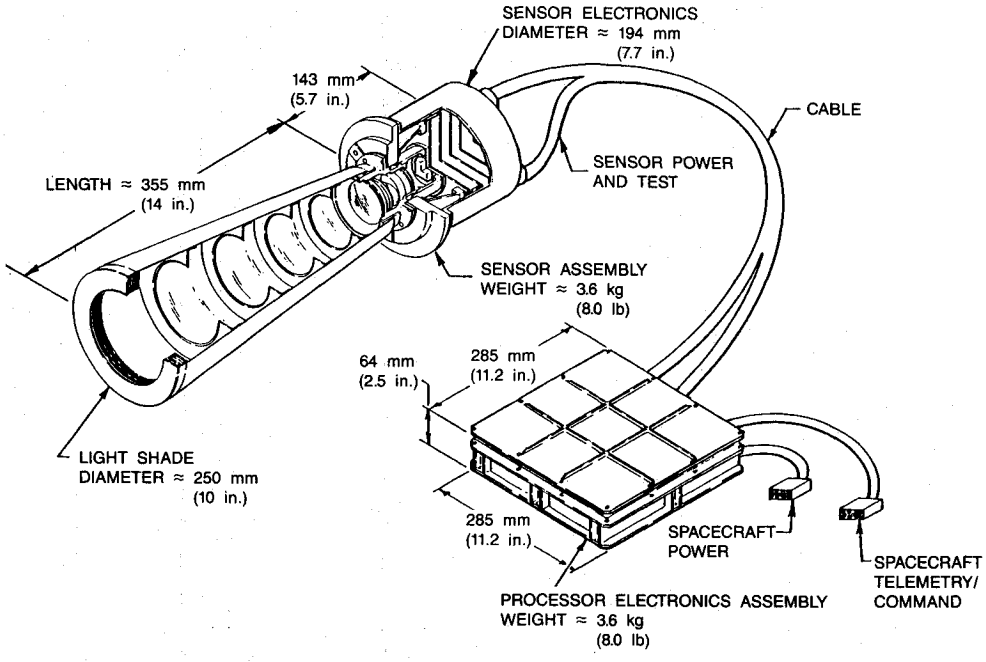

Fig. 5 CID SST.

Table 5 CID SST vs IDT SST physical parameters

Parameter	CID SST	IDT SST
Configuration	Two packages: processor electronics and sensor/shade	Two packages: sensor/electronics and shade/shutter
Volume, in.^{3}	Total system: 1,300 Sensor/shade: 1,000 Processor electronics: 300	Total system: 2,400 Shade/shutter: 1,800 Sensor/electronics: 600
Weight, lb	Total system: 16 Sensor/shade: 8 Processor electronics: 8	Total system: 21 Shade/shutter: 4 Sensor/electronics: 17
Power (W) from 28V S/C bus	12	16 21 (with shutter closed)

the thermal and structural integrity of the sensor components for the necessary arc sec accuracy.

Table 5 compares the physical characteristics of the two-package CID SST to the IDT SST. Both configurations include a light shade that allows tracking of stars to within 40 and 25 deg of the sun and earth limb, respectively, A precision-lapped, classical three-point mount is the mechanical interface for the spacecraft attitude control platform or equivalent mounting surface. The mounting plane is closer to the sensor center of gravity than was possible on the IDT SST, a factor that should improve ruggedness and stability. Although the total system power is 25% less in the CID SST, the power in the sensor area is nearly three times less, a factor that will improve thermal stability and reduce temperature at the CID. It is conceivable that in many applications the sensor/shade assembly can be passively cooled, eliminating the need for a thermoelectric cooler and thereby reducing power dissipation in the sensor unit by another 2 W (30%). Reduction in shade size allows greater flexibility in mounting the shade. Thus, for all applications of the IDT SST, the size and weight of the shade required mounting to the spacecraft bench rather than the tracker to preclude stress-related instabilities. The size of the equivalent CID SST shade allows integration with the sensor, as shown in Fig. 5.

As Fig. 6 shows, the CID SST functions under the control of a microprocessor that executes unique algorithms. An image of the star covers several pixels and is located by sequential sampling of the pixels, which are addressed through horizontal and vertical shift registers along edges of the CID. A basic data block of 4×4 pixels can be selected with one address code. The 16 pixels within this block can then be read independently, summed by columns and rows, or differenced by columns or rows. The address system and on-chip processing are used to duplicate the full FOV acquisition, reduced FOV acquisition, and track modes presently available in the IDT SST.

The full FOV acquisition is accomplished by a sequential sampling of the signal from blocks of 4×4 pixels over the total 256×256 detector. Two time-separated, NDRO readings of each block are taken and subtracted to eliminate repetitive fixed pattern noise. These are then stored in a coarse map that is subsequently searched for a signal exceeding a commanded threshold. Tracking is commenced at the pixel block where threshold is exceeded. The total FOV search requires 5 s. Stars moving at rates up to 0.3 deg/s would be acquired with a probability greater than 95%.

Reduced FOV acquisition would be accomplished by the same 4×4 block reading sequence and signal processing as for the full FOV; however, the reduced area within the full FOV could be selected by the user. To duplicate the present IDT SST offset mode, the CID SST reduced FOV would be approximately 1.25 deg square.

The acquisition modes described previously duplicate the present IDT SST capability but do not illustrate the adaptability afforded by the address system and on-chip processing of the CID. Following are several options that could be accommodated by uncomplicated algorithm changes and that

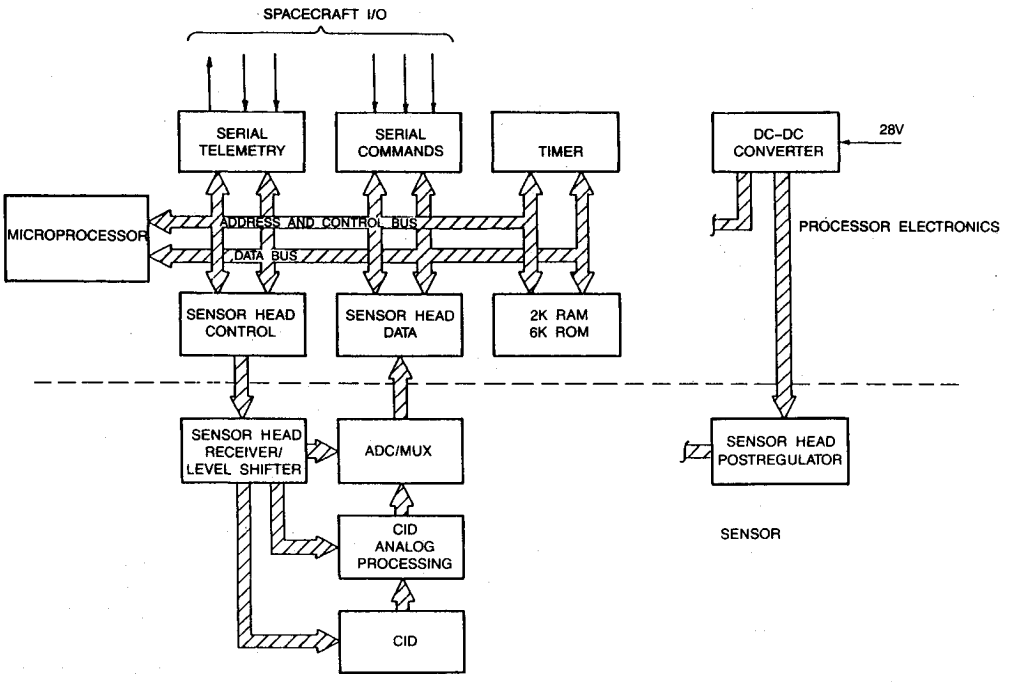

Fig. 6 CID SST electronics.

Table 6 CID SST vs IDT SST performance

Parameter	CID SST	IDT SST	Comment
FOV (deg)	5.8×5.8	8.0 dia	Provide same probability of having trackable star in quality FOV
Sensitivity (M_I)	6.05	5.7	
Full FOV scan time (s)	<5	<11	
Offset FOV (deg)	1.25×1.25	1.75×1.75	
Scan time (s)	<0.3	<0.6	
Star rate (deg/s)	≤0.3	≤0.3	
Probability of acquisition in one scan	>0.95	>0.95	
Data rate (per s)	10	10	Star position and intensity bits per each coordinate
Position data (bits)	14	12	
Accuracy (arc sec)			
Noise equivalent angle	5.7	16	
Interpolation	1.6	0	
Quantization	0.4	2	
Geometric distortion	1.9	≤10	IDT accuracy is after application of calibration equations; CID accuracy is at the device output terminals
Star color	1		
Magnetic field	0		
Thermal	<5		
Launch stability	<5	<10	

might improve sensor performance for a particular mission:

1) Spiral full FOV acquisition scan to ensure tracking stars closer to boresight;

2) Edge search to pick up stars that always move into FOV from one direction, which decreases acquisition time, allows acquisition of faster moving stars, and allows longest time for tracking of stars;

3) Commandable reduced FOV size.

Once the star has been acquired, a track loop is closed so that the set of pixels closest to the image center is continuously sampled. As the image moves, the track algorithm, as executed by the microprocessor, changes the CID addresses to sample the correct pixels. In addition, the microprocessor executes centroiding algorithms operating on pixels' signals adjacent to the image to calculate the relative displacement of the radiometric center of the image from the center pixel. The tracker provides star position and intensity data during the track mode.

Should it be an advantage, a CID tracker could be configured to track and output position and intensity data for multiple stars simultaneously. It is also possible to continually perform a full (or partial) FOV search while tracking stars.

Table 6 compares the performance parameters of a CID SST to an IDT SST. Two points about the comparison are noted and further discussed in subsequent paragraphs: 1) The CID SST sensitivity and FOV provide probability of obtaining trackable stars equal to that of the IDT SST; 2) The CID SST provides better than 10 arc sec accuracy (1σ) at its terminals, whereas the IDT SST position data must be averaged and calibrated external to the tracker to achieve equivalent accuracy.

FOV/Sensitivity Trade-Offs

Numerical integration of the spectral response of the CID and the present SST image dissector tube S-20 photocathode over stellar spectral curves for approximately the 1700

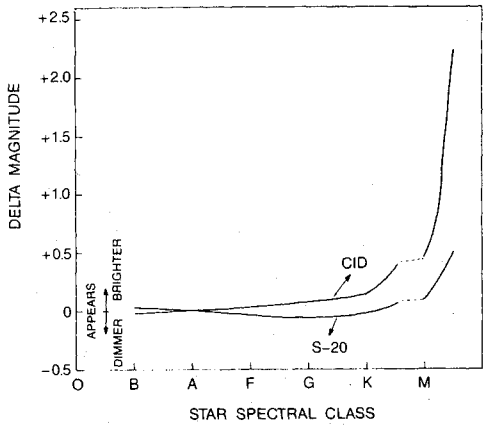

Fig. 7 Instrument color index.

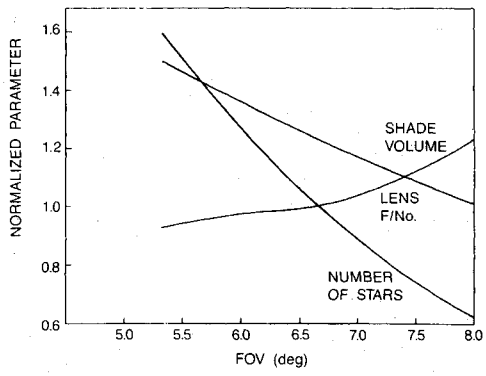

Fig. 8 Tracker parameters vs FOV.

brightest stars provides a comparison of instrument magnitude as a function of stellar spectral class (Fig. 7). The increased red CID sensitivity increases the total number of stars visible at all magnitudes by roughly 20%, which is equivalent to being 0.1 magnitude more sensitive than the SST. The SST, with a sensitivity of 5.7 visual magnitude Class AO star and usable FOV of 8 deg circular, has probability of 0.98 and 0.93 of seeing one and two stars, respectively.

A range of CID SST FOV/sensitivity combinations will provide trackable star probabilities equal to the SST. FOV's that exceed an optimal value allow a need for less sensitivity but impose more stringent demands for interpolation from the CID centroid measurement algorithm and inevitably lead to larger noise equivalent angles and reduced accuracy. FOV's that are smaller than optimal improve accuracy because of less stringent demands on interpolation, but they lead to larger star catalogs, greater sensitivity, and larger, heavier objective lenses. Because of advantages previously stated, the detector chosen for the CID SST is the ST-256. To use the total detector, the different FOV's are accomplished by using optics having different focal lengths. To maintain a constant accuracy (combination of pixel interpolation error and a temporal noise equivalent angle) independent of FOV the optics diameter must be changed. Sensitivity of various parameters, as a function of FOV and CID SSTs, having equal probability of a star in the FOV and equal accuracy as defined above are shown in Figure 8. The fact that the parameters show increasing or decreasing trends rather than a peak or trough indicates selection of the FOV is a fairly soft decision with a need for additional hardware factors to be considered.

Choosing a CID SST field of view of 5.8 deg allows use of 50 mm, f/1.4 refractive optics. Although f/1.0 may be a practical limit, the ease of both lens design and manufacturing increases dramatically with f/number. Performance, specifically chromatic aberration correction which directly affect accuracy, is easier to achieve with fewer elements. As shown in Fig. 8, choice of the smaller FOV provides a slight weight advantage when considering both lens and shade at the expense of needing a larger star catalog. The larger star catalog is only a disadvantage if carried on-board, although the weight needed for another 20% of memory is probably not equivalent to that saved in shades and lenses of several trackers.

Calibration Support Comparisons

Ten-arc-second accuracy is achievable in a wide FOV IDT tracker only by calibration. By themselves, the errors due to field distortion, temperature, star intensity, and magnetic field are much too great to even approach the accuracy wanted.

Fortunately the effect of these variables, being stable and predictable, allows use of calibration to reduce the errors to less than 10 arc-seconds. Each IDT SST is delivered with a unique set of two 20-term calibration equations (one for each coordinate). A user must provide roughly 1,500 bytes of memory per tracker to accommodate calibration. If the magnetic field is >0.5 gauss, the user must also provide a measure of the field to effect calibration for that disturbance.

It is anticipated that some calibration for field distortion and temperature will be required in the CID SST. However, both aberrations will be small enough so that calibration will be accomplished within the device itself. The CID is not magnetically susceptible, and laboratory tests have proven insensitivity to star intensity. Therefore, accuracy of the CID SST is available at the device terminals and no additional data manipulation is necessary.

Conclusions

The operation and performance of the RFT has demonstrated the power of the CID detector-microprocessor combination as an electro-optical sensor. Its success in providing 100% of the data as the sensor of the Solar Array Experiment on STS 41D in August 1984 will lead the way for flight applications of other CID detector star sensors. One of these most certainly will be a CID SST comparable to that described in this paper. With a microprocessor, the tracker will be adaptable to special mission requirements. The CID's inherent detector accuracy will provide accuracy at the tracker terminals greater than that which is available on present trackers with external calibration. For applications where accuracy is not the driving performance parameter (such as the Shuttle Vehicle Guidance and Navigation star trackers and the sounding rocket payload star trackers), the increased accuracy will improve the design margin and reduce manufacturing and testing efforts. For applications where pointing control and attitude determination accuracies are more precise, the CID tracker promises to meet the needed accuracy requirements.

References

[1]Kollodge, J. C. and Sand, J. A., "An Advanced Star Tracker Design Using the Charge Injection Device," *Joint IFAC/ESA Symposium on Automatic Control in Space,* Noordwijkerhout, The Netherlands, July 5-9, 1982.

[2]Burke, H. K. et al., *Design Fabrication and Delivery of Charge Injection Device as a Stellar Tracking Device,* NASA/MSFC Contract NAS8-32801 SRO-78-171, April 1979.

[3]Gutshall, R. L. and Deters, R. A., "A Survey of Attitude Sensors," *Journal of the Astronautical Sciences,* Vol. XXVII, No. 3, July-Sept. 1979, pp. 217, 238.

[4]Cleavinger, R. L. and Mayer, W. F., "Attitude Determination Sensor for Explorer 53," AIAA 14th Aerospace Sciences Meeting, Washington, D.C., Jan. 26-28, 1975.

[5]Deters, R. A., "A User's Guide for the Standard Star Tracker," American Astronautical Society's Annual Guidance and Control Conference, Keystone, CO, Feb. 24-28, 1979.